THE UNIVERSITY of EDINBURGH

Edinburgh Research Explorer

Antiviral RNA Interference Responses Induced by Semliki Forest Virus Infection of Mosquito Cells: Characterization, Origin, and Frequency-Dependent Functions of Virus-Derived Small Interfering RNAs

Citation for published version:
Siu, RWC, Fragkoudis, R, Simmonds, P, Donald, CL, Chase-Topping, ME, Barry, G, Attarzadeh-Yazdi, G, Rodriguez-Andres, J, Nash, AA, Merits, A, Fazakerley, JK & Kohl, A 2011, 'Antiviral RNA Interference Responses Induced by Semliki Forest Virus Infection of Mosquito Cells: Characterization, Origin, and Frequency-Dependent Functions of Virus-Derived Small Interfering RNAs' Journal of Virology, vol 85, no. 6, pp. 2907-2917. DOI: 10.1128/JVI.02052-10

Digital Object Identifier (DOI):
10.1128/JVI.02052-10

Link:
Link to publication record in Edinburgh Research Explorer

Document Version:
Peer reviewed version

Published In:
Journal of Virology

Publisher Rights Statement:
Copyright: American Society for Microbiology

General rights
Copyright for the publications made accessible via the Edinburgh Research Explorer is retained by the author(s) and / or other copyright owners and it is a condition of accessing these publications that users recognise and abide by the legal requirements associated with these rights.

Take down policy
The University of Edinburgh has made every reasonable effort to ensure that Edinburgh Research Explorer content complies with UK legislation. If you believe that the public display of this file breaches copyright please contact openaccess@ed.ac.uk providing details, and we will remove access to the work immediately and investigate your claim.

OPEN ACCESS

Download date: 28. Apr. 2017

JOURNAL OF VIROLOGY, Mar. 2011, p. 2907–2917 Vol. 85, No. 6
0022-538X/11/$12.00 doi:10.1128/JVI.02052-10
Copyright © 2011, American Society for Microbiology. All Rights Reserved.

Antiviral RNA Interference Responses Induced by Semliki Forest Virus Infection of Mosquito Cells: Characterization, Origin, and Frequency-Dependent Functions of Virus-Derived Small Interfering RNAs▽†

Ricky W. C. Siu,[1] Rennos Fragkoudis,[1] Peter Simmonds,[1] Claire L. Donald,[1] Margo E. Chase-Topping,[1] Gerald Barry,[1] Ghassem Attarzadeh-Yazdi,[1] Julio Rodriguez-Andres,[1] Anthony A. Nash,[1] Andres Merits,[2] John K. Fazakerley,[1]* and Alain Kohl[1]*

The Roslin Institute and Centre for Infectious Diseases, University of Edinburgh, Edinburgh EH9 1QH, Scotland, United Kingdom,[1] *and Institute of Technology, University of Tartu, Nooruse 1, Tartu 50411, Estonia*[2]

Received 28 September 2010/Accepted 20 December 2010

RNA interference (RNAi) is an important mosquito defense mechanism against arbovirus infection. In this paper we study the processes underlying antiviral RNAi in *Aedes albopictus*-derived U4.4 mosquito cells infected with Semliki Forest virus (SFV) (*Togaviridae*; *Alphavirus*). The production of virus-derived small interfering RNAs (viRNAs) from viral double-stranded RNA (dsRNA) is a key event in this host response. dsRNA could be formed by RNA replication intermediates, by secondary structures in RNA genomes or antigenomes, or by both. Which of these dsRNAs is the substrate for the generation of viRNAs is a fundamental question. Here we used deep sequencing of viRNAs and bioinformatic analysis of RNA secondary structures to gain insights into the characteristics and origins of viRNAs. An asymmetric distribution of SFV-derived viRNAs with notable areas of high-level viRNA production (hot spots) and no or a low frequency of viRNA production (cold spots) along the length of the viral genome with a slight bias toward the production of genome-derived viRNAs over antigenome-derived viRNAs was observed. Bioinformatic analysis suggests that hot spots of viRNA production are rarely but not generally associated with putative secondary structures in the SFV genome, suggesting that most viRNAs are derived from replicative dsRNA. A pattern of viRNAs almost identical to those of *A. albopictus* cells was observed for *Aedes aegypti*-derived Aag2 cells, suggesting common mechanisms that lead to viRNA production. Hot-spot viRNAs were found to be significantly less efficient at mediating antiviral RNAi than cold-spot viRNAs, pointing toward a nucleic acid-based viral decoy mechanism to evade the RNAi response.

Arboviruses are transmitted to vertebrates by arthropods such as mosquitoes or ticks (58, 59). The genus *Alphavirus* within the family *Togaviridae* contains medically important mosquito-borne arboviruses such as chikungunya virus and Venezuelan equine encephalitis virus (42, 59). The replication of the prototype alphaviruses Sindbis virus (SINV) and Semliki Forest virus (SFV) in vertebrate cells is well understood (19, 23, 45). The alphavirus genome is a positive-stranded RNA with a 5′ cap and a 3′ poly(A) tail. The 5′ two-thirds encodes the nonstructural polyprotein P1234, which is separated into four replicase proteins, nsP1 to nsP4, by proteolytic cleavage; during replication, the genome is transcribed into a full-length copy (the antigenome), which in turn serves as a template for the *de novo* transcription of viral genomes (32, 34, 57). The 3′ one-third encodes the structural polyprotein, which is translated from a subgenomic mRNA and generates the capsid and envelope glycoproteins after proteolytic processing (54). Alphaviruses replicate within cytoplasmic replication complexes associated with cellular membranes, and viruses mature by budding (17, 45); important differences in replication complex formation between vertebrate and mosquito cells have been described (16). The infection of mosquito cell cultures with alphaviruses usually starts with an acute phase characterized by efficient virus production, followed by the establishment of a persistent infection with low-level virus production (6, 10, 15).

The efficient control of arbovirus infection in insects such as mosquitoes is believed to be due to innate immune responses, and alphaviruses such as SFV have proven to be good models to study these responses (14). The best-characterized mosquito antiviral defense system to date is RNA interference (RNAi) (14, 47), which controls arbovirus replication, spread, and transmission (26, 46). Central to antiviral RNAi in insects is the production of virus-derived small interfering RNAs (viRNAs) from viral double-stranded RNA (dsRNA) and the assembly of an RNA-induced silencing complex (RISC), followed by the degradation of target single-stranded viral RNA in a sequence-dependent manner (14, 25). The origin of the dsRNA substrate is not clear and could involve double-stranded regions in single viral genome or antigenome RNA molecules or two-molecule replication intermediates (the favored hypothesis) (38). Mosquito orthologues of the *Drosophila melanogaster* RNAi proteins Dcr-2, R2D2, and Ago-2 are important for mosquito RNAi responses against flaviviruses and alphaviruses (7, 8, 24, 46). In *D. melanogaster*, the RNase

* Corresponding author. Mailing address: The Roslin Institute and Centre for Infectious Diseases, University of Edinburgh, Edinburgh EH9 1QH, Scotland, United Kingdom. Phone: 44 (0)131 651 3907. Fax: 44 (0)131 650 6511. E-mail for John K. Fazakerley: John.Fazakerley@ed.ac.uk. E-mail for Alain Kohl: Alain.Kohl@ed.ac.uk.

† Supplemental material for this article may be found at http://jvi.asm.org/.

▽ Published ahead of print on 29 December 2010.

III enzyme and DExD/H-box RNA helicase Dcr-2 is a pattern recognition receptor (PRR) which initiates RNAi by the cleavage of virus-derived long dsRNA into double-stranded viRNAs. Dcr-2 and R2D2 interact during the process of viRNA generation and integrate viRNAs into the RISC. One of the viRNA strands (the guide strand; the passenger strand is degraded) is retained within the RISC, which targets and recognizes viral single-stranded RNA in a sequence-specific manner and mediates cleavage through the RISC protein Ago-2 (25). In mosquitoes infected with SINV and o'nyong-nyong virus, the cloning and sequencing of viRNAs showed that viRNA strands are mainly 21 nucleotides (nt) in length. These viRNAs map asymmetrically along the complete length of the virus genome; regions generating a high frequency of viRNAs (hot spots) and regions generating no or a low frequency of viRNA (cold spots) are interspersed in an apparently random manner (38, 39). However, as these infections are nonsynchronized but reflect a mix of cells at various stages of infection, it is difficult to speculate on the origins of viRNAs. It appears that arboviruses do not encode protein suppressors of RNAi, unlike pathogenic insect viruses, many of which encode, for example, dsRNA-binding proteins that counteract RNAi (14, 25). It has been speculated that an RNAi-suppressive activity may exist in dengue virus-infected mosquito cells (46). In addition, it is now known that there is a systemic component to RNAi responses in insects (3, 44). Little is known with regard to the biogenesis of arbovirus-derived viRNAs. In the case of positive-strand RNA viruses or viroids of plants, the predominance of genome-derived viRNAs has led to the suggestion that secondary structures in the genome are the substrate for dicer, although replication intermediates have also been implicated (20, 22, 37, 61). For alphaviruses, this remains a topic of debate, and the substrate for Dcr-2, viral dsRNA, could be replication intermediates, secondary structures, or both (14, 38).

Here we show that a synchronized SFV infection of *Aedes albopictus* cells induced dsRNA, which colocalizes mainly with virus nsP proteins in replication complexes. By using deep sequencing, we observed an asymmetric distribution of SFV-derived viRNAs with areas of high-level viRNA production (hot spots) and no or a low frequency of viRNA production (cold spots) along the length of the viral genome and antigenome, with a slight bias toward the production of genome-derived viRNAs. The infection of *A. albopictus*- and *Aedes aegypti*-derived mosquito cells resulted in almost identical viRNA production patterns. Hot-spot viRNAs, present at a high frequency during infection, were found to have only poor antiviral activity compared to cold-spot viRNAs. This points toward a nucleic acid-mediated RNAi decoy mechanism protecting against antiviral RNAi. Bioinformatic analysis of RNA secondary structures and pairing in the SFV genome (by MFE [minimal free energy]-based thermodynamic large-scale secondary structure prediction and StructureDist pairing/secondary structure prediction) suggests no general correlation between the frequency or location of viRNA generation and putative RNA structures in SFV genomic RNA. This strengthens the hypothesis that the origin and production of alphavirus viRNAs are linked to dsRNA generation during replicative processes rather than secondary structures in the viral genome.

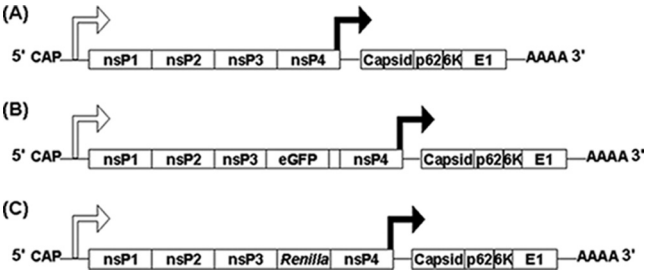

FIG. 1. Viruses used in this study. (A) SFV (prototype strain SFV4). (B) SFV4(3F)-eGFP, encoding the eGFP green fluorescent reporter protein (inserted into to the C-terminal region of nsP3) as part of the viral nonstructural polyprotein. (C) SFV4(3H)-*RLuc*, carrying the *Renilla* luciferase (*RLuc*) reporter gene (flanked by duplicated nsP2-protease cleavage sites at the nsP3/4 junction) as part of the viral nonstructural polyprotein.

MATERIALS AND METHODS

Cells, viruses, and infection. *A. albopictus*-derived U4.4 and *A. aegypti*-derived Aag2 mosquito cells were grown at 28°C in L-15 medium with 10% fetal calf serum and 8% tryptose phosphate broth. The amplification and titration of SFV (strain SFV4) and clones derived from this virus and infection of U4.4 cells were carried out as described previously (3). Briefly, SFV4 or derived recombinant viruses were grown in BHK-21 cells in Glasgow's minimal essential medium (GMEM) with 2% newborn calf serum (37°C in a 5% CO_2 atmosphere). Details of the reporter viruses (Fig. 1) used can be obtained from the authors. Viruses were purified from the supernatant as described previously (12). Virus (resuspended in Tris-NaCl-EDTA [TNE] buffer) was titrated by a plaque assay on BHK-21 cells. For the infection of mosquito cells, viruses were diluted in PBSA (phosphate-buffered saline [PBS] with 0.75% bovine serum albumin); cells were infected at 28°C for 1 h and washed twice to remove any unbound particles.

Transfection of hot-spot/cold-spot-derived viRNA mimic siRNAs. siRNA mimics of SFV viRNAs were produced by Ambion (Table 1). siRNAs for *Renilla* luciferase (*RLuc*) and negative-control siRNA (siRNA 1) were obtained from Ambion (AM4630 and AM4611). Approximately 1.625×10^5 U4.4 or 1.6×10^5 Aag2 cells/well were grown in 24-well plates. Before transfection, the medium was replaced with fresh complete medium. siRNAs (final concentration, 10 nM) were mixed with 1 μl/well Lipofectamine 2000 (Invitrogen) in Optimem according to the manufacturer's instructions. One hundred microliters of the nucleic acid-Lipofectamine 2000 complexes was added to 400 μl of medium in each well and incubated for 5 h at 28°C. After transfection, cells were washed twice to remove liposomes, and complete medium was added. Where indicated, SFV infection was carried out 24 h after siRNA transfection.

Small RNA isolation and deep sequencing. Total RNA was isolated from U4.4 or Aag2 cells by using Trizol (Invitrogen). Approximately 6.5×10^5 U4.4 or 8.6×10^5 Aag2 cells grown in 6-well plates were infected with SFV (multiplicity of infection [MOI] of 10). Total RNA was extracted at 24 h postinfection (p.i.); the concentration and purity were determined by using a NanoDrop 1000 instrument (Thermo Scientific). All subsequent RNA processing was performed at GenePool, University of Edinburgh (http://genepool.bio.ed.ac.uk/). Small RNAs smaller than 44 nt were purified from a 15% Tris-borate-EDTA (TBE)–urea polyacrylamide gel, and RNA adapters were ligated before sequencing according to the manufacturer's instructions (Illumina Inc.). Small RNAs were then sequenced by using an Illumina Solexa genome analyzer. Small RNAs derived from uninfected cells were sequenced as a control. To identify SFV-derived viRNAs, small RNA sequences were compared to the SFV4 reference genome/antigenome sequence (GenBank accession number X04129) corrected by the recent resequencing of SFV4 (GenBank accession number AJ251359) (compiled by A. Merits, personal communication) using SOAP software (with the help of GenePool bioinformatics support) (29). Small RNA data as used in the figures within this paper are shown in Tables S1 to S3 in the supplemental material (Excel tables), which contain viRNA sequences mapping to the SFV genome or antigenome, and both types of viRNAs are separately listed in labeled sheets within each Excel table; + indicates viRNAs mapping to the SFV genome, and − indicates viRNAs mapping to the SFV antigenome (sequences complementary to antigenome viRNAs are shown in a 5′-to-3′ orientation to simplify mapping; the viRNA sequence is a complement, reading from left to right, 3′ to 5′). The viRNA location/starting position on the SFV genome or antigenome (column B

TABLE 1. Sequences and characteristics of siRNA mimics of hot- and cold-spot-derived viRNAs mapping to the SFV genome[a]

siRNA or SFV genome position	Sequence	viRNA frequency (no. of reads) for U4.4 cells/U4.4 cells/Aag2 cells	Relative *RLuc* expression (%) for U4.4 cells/Aag2 cells
Negative-control siRNA[b]		NA	100
Positive-control *RLuc* siRNA[c]		NA	30.5/23.8
1016 (cold)	5′-GAGGGAUUCCUAGUGUGCAAG-3′ 3′-GCCUCCCUAAGGAUCACACGU-5′	0/3/0	21.7/31.2
1268 (hot)	5′-UGGGCGAGGGAAUACAAGGCA-3′ 3′-UCACCCGCUCCCUUAUGUUCC-5′	393/353/253	91.6/103.6
2257 (hot)	5′-UCCGGGAUCAGGCAAGUCUGC-3′ 3′-CAAGGCCCUAGUCCGUUCAGA-5′	341/133/79	60.5/92.7
2460 (cold)	5′-UCGCUUGCCAUUCCGGUACUC-3′ 3′-AAAGCGAACGGUAAGGCCAUG-5′	0/0/0	51.8/36.3
3456 (cold)	5′-UCGCAGAAAGAAAAAUCCAAC-3′ 3′-AUAGCGUCUUUCUUUUUAGGU-5′	0/0/0	20.6/39
3549 (hot)	5′-CGGUUAAAGGCAGUAGGGUUG-3′ 3′-GAGCCAAUUUCCGUCAUCCCA-5′	300/354/261	21.4/42.2
5129 (cold)	5′-GACUCGUCUUCCACUGCCAGC-3′ 3′-GGCUGAGCAGAAGGUGACGGU-5′	0/3/0	39/38.1
6847 (cold)	5′-GUUUAUUAACACUGUUUUGAA-3′ 3′-AACAAAUAAUUGUGACAAAAC-5′	0/2/0	24.7/41.2
7305 (hot)	5′-UGGCGAGGGACAUUAAGGCGU-3′ 3′-GAACCGCUCCCUGUAAUUCCG-5′	397/256/245	94.1/106.1
8340 (hot)	5′-CGAGGAUAACGUGGAUAGGCC-3′ 3′-GAGCUCCUAUUGCACCUAUCC-5′	324/1,039/753	97.5/81.4
9887 (cold)	5′-UGCCGAACGUGGUGGGGUUCC-3′ 3′-UUACGGCUUGCACCACCCCAA-5′	0/0/1	43.7/90.2
10181 (hot)	5′-AGGCGUACGUCGAUCGAUCGG-3′ 3′-GCUCCGCAUGCAGCUAGCUAG-5′	177/848/316	62.2/70.3
10499 (hot)	5′-ACGACCUGUACGCGAACACGG-3′ 3′-AUUGCUGGACAUGCGCUUGUG-5′	252/2,744/1,116	89.7/97.7
10645 (cold)	5′-CAAAUCAAAACGAACCCUGUC-3′ 3′-CGGUUUAGUUUUGCUUGGGAC-5′	0/1/1	81.7/102.4

[a] dsRNA duplexes and locations of viRNAs on the SFV genome are shown; the 5′ nucleotide of the siRNA top strand indicates the start of the corresponding viRNA sequence on the SFV genome. viRNA frequencies (read numbers) in U4.4 (see Tables S1 and S2 in the supplemental material) and Aag2 (Table S3) cells are shown (order of U4.4, U4.4, and Aag2). The average relative *RLuc* activity (indicator for SFV replication) in the presence of a given siRNA relative to a negative-control scrambled siRNA (100% *RLuc* activity) is indicated per cell type (U4.4 or Aag2 cells). NA, not applicable.
[b] AM4611 (Ambion).
[c] AM4630 (Ambion).

in Tables S1 to S3), sequence (column C in Tables S1 to S3), frequency (number of reads; positions from which no viRNA is generated are not shown and are listed as 0 reads in Table 1) (column D in Tables S1 to S3), and length (nt) (column E in Tables S1 to S3) are indicated in each sheet (see Table S1 in the supplemental material for SFV viRNAs from U4.4 cells used in Fig. 3 and 6 and Fig. S2; see Table S2 in the supplemental material for SFV viRNAs from U4.4 cells used in Fig. 5 and Fig. S1 and S2; and see Table S3 in the supplemental material for SFV viRNAs from Aag2 cells used in Fig. 4 and 5 and Fig. S1).

Luciferase assays. Cells were lysed in passive lysis buffer (Promega), and *Renilla* luciferase (*RLuc*) activities were measured by using a dual-luciferase assay (Promega) with a GloMax 20/20 luminometer.

RNA secondary structure prediction. The existence and position of RNA secondary structures in SFV genomic RNA were predicted by thermodynamic folding energy calculations that used comparative sequence data from the available SFV complete genome sequences (SFV4 as described above and GenBank accession numbers EU350586, DQ189086, and Z48163). This analysis was performed by using the program UNAFold (62). For calculations of folding energies, sequences in the SFV alignment were split into sets of 150 base fragments incrementing by 1 base across the genome. Folding energies were compared with those of 50 copies of each fragment whose sequence order was scrambled using the algorithm NDR, which preserves dinucleotide frequencies of the native sequence automated using the program Folding Energy Scan as implemented in the Simmonic2005 v1.8 package (50). The minimum free energies (MFEs) of each native sequence fragment were compared with the mean MFE of the NDR-scrambled controls to produce an MFE difference (MFED) as previously described (51). MFED values for each fragment were averaged across the 4 available SFV complete genome sequences.

The prediction of specific structures using the available comparative sequence

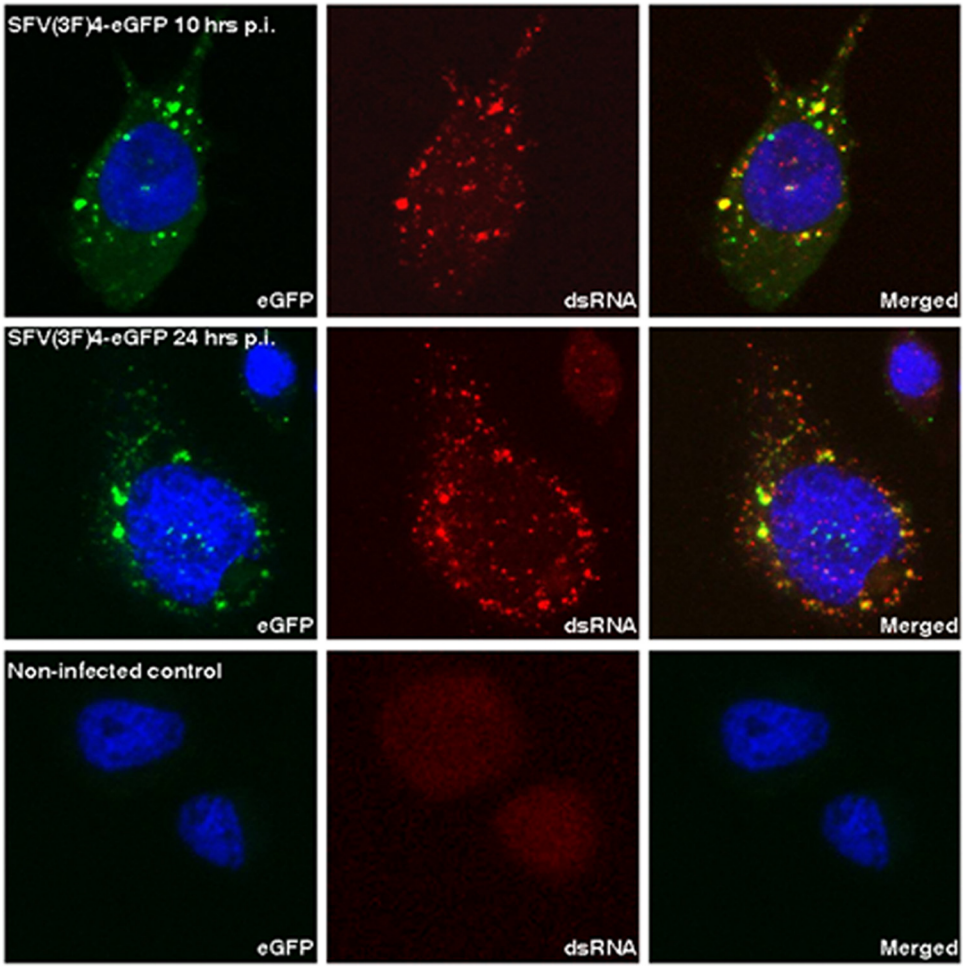

FIG. 2. SFV-induced dsRNA is present in mosquito cells and colocalizes with vesicular replication complexes. *A. albopictus*-derived U4.4 mosquito cells were mock infected or infected with SFV4(3F)-eGFP (in which eGFP is fused to nsP3) (Fig. 1). The green signal marks complexes made by nsP3-eGFP, including virus replication complexes. Cells were fixed at 10 or 24 h p.i. dsRNA (red signal) was revealed by immunostaining with dsRNA-specific antibody J2; cell nuclei were labeled with To-Pro3.

data for SFV was done by using the program StructureDist in the Simmonics package. This program compares minimum energy structures from sequence data sets and computes phylogenetically conserved pairings and secondary structures. The results were expressed in the form of pairing frequencies, which is calculated from the proportion of pairwise comparisons of connect files for each sequence with the same pairing predictions, as previously described (51).

Immunostaining. U4.4 cells were fixed with 4% paraformaldehyde. After 2 washes (in PBS), cells were permeabilized with 0.3% Triton X-100 in PBS for 20 min and washed twice. After blocking with CAS block (Invitrogen), J2 antibody (Scicons, Hungary) (in CAS block; 1:400) was added, followed by three washes. Incubation with secondary antibody (sheep anti-mouse biotinylated IgG [Vector Labs] in CAS block) was followed by three washes before the addition of streptavidin-conjugated Alexa Fluor 594. After a further two washes, slides were mounted with mounting medium (Vector Laboratories), and images were acquired (Zeiss AxioSkop confocal microscope).

RESULTS

SFV infection-induced dsRNA colocalizes with virus replication complexes. U4.4 mosquito cells have functional antiviral immune responses and resemble infectivity of the mosquito; the acute phase of SFV infection in these cells lasts up to 24 h postinfection (p.i.) (3, 15, 35). dsRNA is produced in SINV-infected mammalian and mosquito cells (53). To determine the relationship between alphavirus replication complexes and dsRNA (the trigger of immune responses) in mosquito cells, *A. albopictus*-derived U4.4 cells were infected with recombinant SFV4 encoding an nsP3-enhanced green fluorescent protein (eGFP) fusion protein, SFV(3F)4-eGFP (55) (Fig. 1). The nsP3-eGFP fusion marks (although not exclusively) viral replication complexes. At 10 and 24 h p.i., cells were stained with anti-dsRNA antibody J2, which recognizes dsRNA of more than 40 bp in length (48, 60). The nsP3-eGFP fusion protein and dsRNA colocalized into punctate cytoplasmic complexes (Fig. 2) throughout the acute phase of infection, a distribution consistent with virus replication on cytoplasmic vacuoles as described previously for the replication of SFV and other alphaviruses in vertebrate and invertebrate cells (15, 16, 45, 52). This shows that the substrates for dsRNA pattern recognition are localized predominantly to virus replication vesicles.

The SFV-induced antiviral RNAi response: characterization and analysis of viRNAs. SFV-derived viRNAs generated during the infection of *A. albopictus*-derived U4.4 cells were characterized at 24 h p.i. by deep sequencing. At an MOI of 10, all cells in the culture were infected with SFV synchronously; this

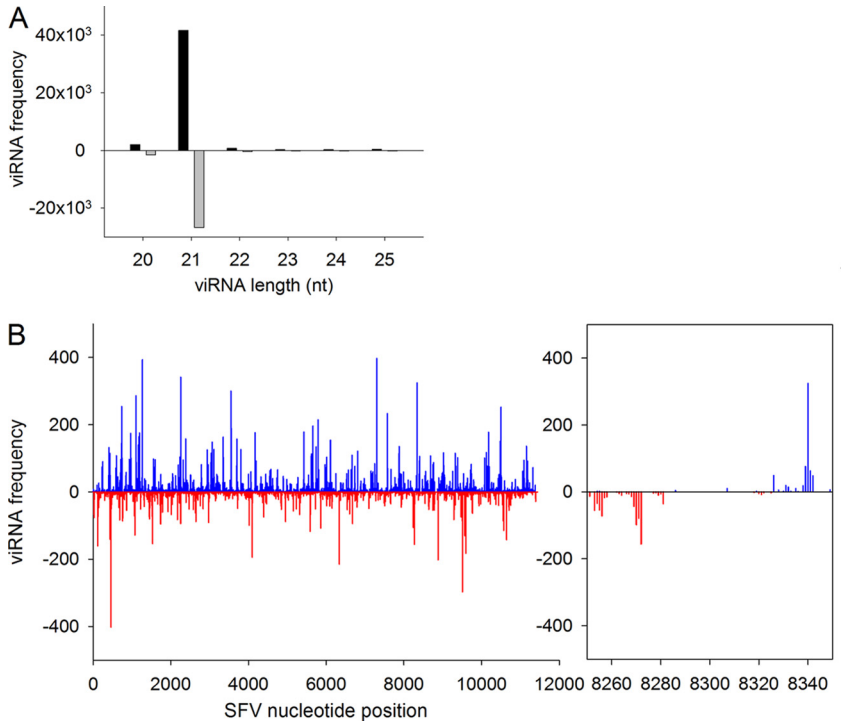

FIG. 3. Characteristics of SFV-derived viRNAs in *A. albopictus*-derived U4.4 cells at 24 h p.i. (A) Size distribution of viRNAs in SFV-infected U4.4 cells at 24 h p.i. Positive numbers on the *y* axis indicate the frequency of viRNAs mapping to the SFV genome (black boxes); negative numbers on the *y* axis indicate the frequency of viRNAs mapping to the SFV antigenome (gray boxes). (B) Frequency distribution of 21-nt viRNA-generating loci in the SFV genome (5′ to 3′; viRNAs starting with the 5′ terminal nucleotide) or antigenome (3′ to 5′; viRNAs starting with the 3′ terminal nucleotide), starting at nucleotide 1 on the *x* axis. Numbers on the *y* axis correspond to the frequencies of viRNAs mapping to the SFV genome (positive) or antigenome (negative). Blue peaks indicate loci of viRNAs mapping to the SFV genome, and red peaks indicate loci of viRNAs mapping to the SFV antigenome. A representative section is magnified (right) to highlight hot and cold spots in more detail. Virtually no (131 SFV genome reads and 76 antigenome reads) sequences from uninfected control cells aligned to the SFV genome.

is different from the infection of live mosquitoes, where a mix of viRNAs from cells at different stages of infection is obtained. RNA molecules below 44 nt were isolated for analysis; the sequences, frequencies, and locations of viRNAs mapping to the SFV genome or antigenome described in this and subsequent experiments are indicated in Tables S1 to S3 in the supplemental material (see Materials and Methods). In total, 3.2×10^6 small RNA sequences were generated, of which 2.1% aligned to the SFV sequence. SFV-derived viRNAs were found to be predominantly 21 nt in length; 21-nt viRNAs accounted for 91.7% of 21- to 25-nt sequences (see Table S1 in the supplemental material for details of viRNAs). A total of 55.8% of the 21-nt viRNAs mapped to the SFV genome, and 35.9% mapped to the virus antigenomic RNA (Fig. 3A). The 21-nt viRNAs were scattered over the entire SFV genome and antigenome with a variable frequency (Fig. 3B). Some areas generated high frequencies of viRNAs (hot spots), and others generated no (or only very few) viRNAs (cold spots). The distribution of viRNAs mapping to the genome and antigenome appeared largely asymmetric. Sequence analysis of SFV-aligned viRNAs indicated no obvious skewing toward a particular base at the first position (28% A, 28% C, 12% G, and 32% U), no bias in GC content, and no obvious common sequence motifs. The same pattern was generated for the SFV replicon region when cells were infected with virus replicon particles (not shown).

To determine if the host species influences viRNA generation, an identical study was performed with *A. aegypti*-derived Aag2 cells. Aag2 cells were previously shown to mount an RNAi response to dengue virus infection (46). SFV replicated to lower titers in Aag2 cells but had a temporal profile of infectious virus production similar to that which we have described previously for U4.4 cells (15). SFV-derived viRNA sequences in Aag2 cells were determined as described above for U4.4 cells (see Table S3 in the supplemental material for viRNA data). A total of 97.6% of viRNAs were 21 nt in length, similar to U4.4 cells (see above), and the majority of these viRNAs (58.2%) mapped to the SFV genome, and 39.4% mapped to the antigenome (Fig. 4A). Again, a very noticeable distribution of hot- and cold-spot viRNA generation was observed (Fig. 4B). SFV viRNAs obtained from U4.4 cells (as described in Fig. 3 but from an independent experiment [Table S2]) were analyzed at the same time as Aag2 viRNAs. The distribution and profiles of U4.4 cell-derived viRNAs mapping to the SFV genome or antigenome were compared to Aag2 cell-derived viRNAs mapping to the SFV genome or antigenome, respectively. As shown in Fig. 5 (also see Fig. S1 in the supplemental material), patterns of viRNAs mapping to the SFV genome or antigenome were largely identical for the two cell types, indicating that the generation of viRNAs is remarkably conserved between these two cell types from related but different species. As expected, a direct comparison of viRNAs

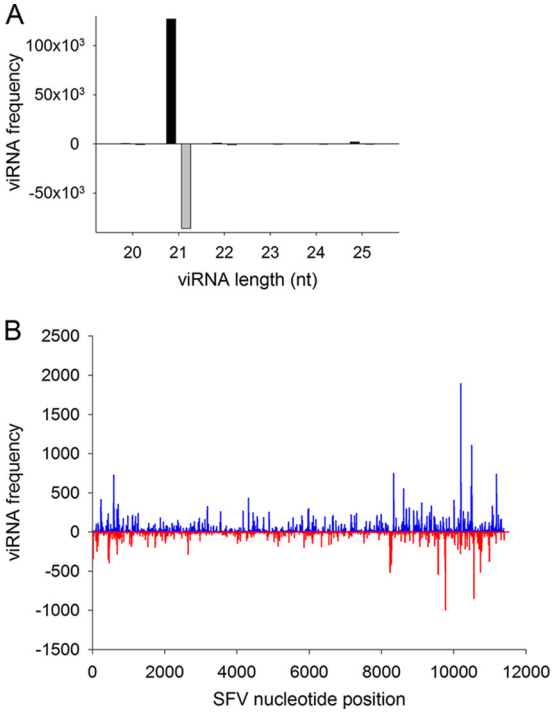

FIG. 4. Characteristics of SFV-derived viRNAs in *A. aegypti*-derived Aag2 cells at 24 h p.i. (A) Size distribution of viRNAs in SFV-infected Aag2 cells at 24 h p.i. Positive numbers on the *y* axis indicate the frequency of viRNAs mapping to the SFV genome (black boxes); negative numbers on the *y* axis indicate the frequency of viRNAs mapping to the SFV antigenome (gray boxes). (B) Frequency distribution of 21-nt viRNA-generating loci in the SFV genome (5′ to 3′; viRNAs starting with the 5′ terminal nucleotide) or antigenome (3′ to 5′; viRNAs starting with the 3′ terminal nucleotide), starting at nucleotide 1 on the *x* axis. Numbers on the *y* axis correspond to frequencies of viRNAs mapping to the SFV genome (positive) or antigenome (negative). Blue peaks indicate loci of viRNAs mapping to the SFV genome, and red peaks indicate loci of viRNAs mapping to the SFV antigenome.

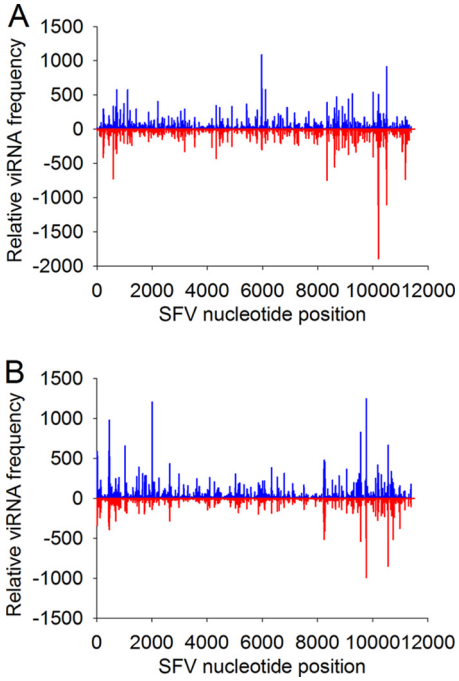

FIG. 5. Comparative analysis of SFV viRNA distribution profiles from *A. albopictus*-derived U4.4 cells and *A. aegypti*-derived Aag2 cells at 24 p.i. The *x* axis represents the SFV genome (5′ to 3′) (A) or antigenome (3′ to 5′) (B), starting at nucleotide 1. For better comparisons of viRNA distribution along the SFV genome/antigenome loci in two cell types, viRNA frequencies for each cell type were normalized to their median 50% value (a comparison of the original distribution and frequencies is shown in Fig. S1 in the supplemental material). (A) Comparative analysis of viRNAs mapping to the SFV genome. The *y* axis represents relative viRNA frequencies (positive, U4.4 cell-derived viRNAs; negative, Aag2 cell-derived viRNAs). Blue peaks represent U4.4 cell-derived viRNA loci; red peaks represent Aag2 cell-derived viRNA loci. (B) Comparative analysis of viRNAs mapping to the SFV antigenome. The *y* axis represents relative viRNA frequencies (positive, U4.4 cell-derived viRNAs; negative, Aag2 cell-derived viRNAs). Blue peaks represent U4.4 cell-derived viRNA loci; red peaks represent Aag2 cell-derived viRNA loci.

from both U4.4 experiments (Tables S1 and S2) also shows that the patterns and locations of viRNA hot spots and cold spots are highly conserved between experiments, although read frequencies can vary (Fig. S2).

Structural analysis of SFV genomic RNA and role of RNA structures in viRNA generation. Previous work with plant-infecting, positive-strand RNA viruses or viroids suggested that double-stranded structures in the viral RNA can generate viRNAs (20, 22, 36, 61). Little is known about the existence of RNA structures in SFV genomic RNA; alphavirus genomes are predicted to be mainly unstructured (11). However, structures in the 5′ untranslated region of Venezuelan equine encephalitis and Sindbis viruses, which influence replication in mosquito cells, have been described (28, 40); structures in the 5′ untranslated region have been predicted for all alphaviruses (41); and stem-loop structures in the SFV 5′ untranslated region have been identified (30).

The secondary structure within the SFV genome was predicted by using large-scale thermodynamic prediction of minimal free energy (MFE) (50). MFE results are expressed as MFE differences (MFED), that is, the percentage difference between the MFE of the native sequence and the mean of a scrambled control of the same sequence: MFED (%) = $[(MFE_{native}/MFE_{scrambled}) - 1] \times 100$.

The MFED value provides a scale to quantify sequence order-dependent RNA structure formation over the length of the genome. Values plotted in Fig. 6A represent mean values of five consecutive fragments. All nucleotide positions were calculated relative to the SFV4 sequence.

As shown in Fig. 6A, MFED values approximate zero (equal to or just above or below zero) for most of the SFV genome (indicating an absence of structured RNA), with some exceptions, including the previously predicted region of known secondary structure at the 5′ end. We compared the frequency distribution of 21-nt genome-derived viRNAs (as shown in Fig. 3) with the pairing and MFED values (Fig. 6A). Statistical tests to analyze the relationship between MFED values and viRNA frequencies were done by using analysis of variance (ANOVA) (Minitab, version 15) after categorizing viRNA frequencies as follows: 1, <10, 10 to 100, and >100. The results showed that there are no significant differences in MFED values across all

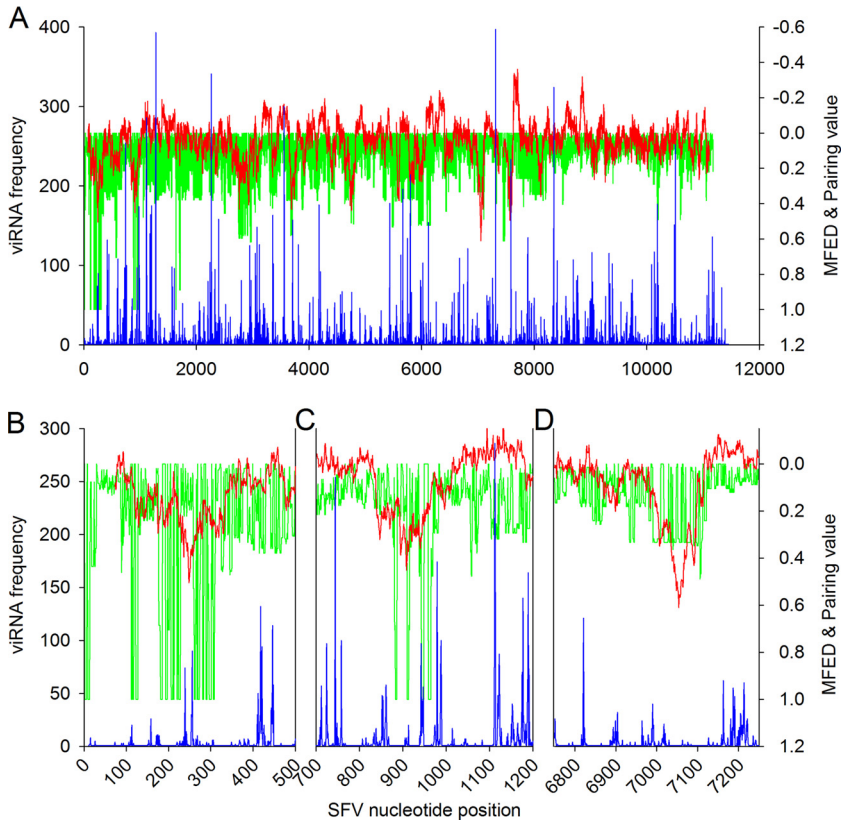

FIG. 6. (A) Prediction of RNA secondary structures and pairing within the SFV genome by MFED and StructureDist bioinformatic analysis and correlation to the 21-nt viRNA frequency in U4.4 cells. viRNAs described in the legend to Fig. 3 were used for this analysis. The distribution of MFED and pairing values (right *y* axis) along the SFV genome (*x* axis, starting at nucleotide 1) are shown as a red line and green shadow, respectively. High positive MFED values suggest areas with RNA secondary structures, while values around 0 or negative do not. Pairing values close to or equal to 1 suggest paired regions and secondary structures, whereas low pairing values indicate an absence of pairing. For the clarity of the figure, ascending values on the right *y* axis are indicated from top to bottom. viRNA frequencies on locations along the SFV genome (blue peaks) are indicated on the left *y* axis. (B, C, and D) Magnifications of selected regions from A.

designated levels of viRNAs ($F = 0.56$; df = 3, 10,882; $P = 0.643$). Secondary structures and paired regions (high probability of pairing indicated by values close or equal to 1) in the SFV4 genome were predicted by using StructureDist (Fig. 6A). The relationships between pairing values and viRNA frequencies were analyzed by using Fisher's exact tests (StatXact v8; Cytel Software Corp., Cambridge, MA). viRNA frequencies were placed into 4 categories (as described above). The pairing values were categorized above or below cutoff values of 0.4 or 0.6 in two separate tests. The results show that there is no significant association between pairing values and levels of viRNAs ($P = 0.286$ for a cutoff of 0.4; $P = 0.1147$ for a cutoff of 0.6).

Whereas there were no correlations across the whole data set, there were nonetheless specific regions where predicted secondary structures in the genome RNA were associated with interesting viRNA patterns. Very high viRNA frequencies were consistently (between experiments and cell types) associated with a genome region (nucleotides 204 to 258) between two stem-loop structures (stem-loops with pairing values close or equal to 1 indicated by green peaks in Fig. 6B; also represented in Fig. 7) predicted by using Mfold (33, 63). Clearly, a high viRNA frequency does not always coincide with high pairing or MFED values (Fig. 6B and C). A long-distance pairing analysis of the genome identified 22 regions with complementary sequences which could allow folding back to form secondary structures. Analysis of the viRNA frequency indicated that these regions produced no viRNAs or only a low frequency of viRNAs.

siRNA mimics of hot-spot- and cold-spot-derived viRNAs differ in their abilities to inhibit SFV replication. The ability to interfere with virus replication of 21-nt siRNAs matching hot or cold spots on the SFV genome (see Table 1 for sequences, genome locations, and frequencies) was tested by using SFV expressing a *Renilla* luciferase (*RLuc*) reporter gene, SFV4(3H)-*RLuc* (Fig. 1). This reporter virus encoded *RLuc* (flanked by duplicated nsP2-protease cleavage sites at the nsP3/4 junction) as part of the viral nonstructural polyprotein; *RLuc* activity is an accurate readout for SFV replication, virus production, and spread in mosquito cells (3, 15, 27). siRNA mimics of viRNAs were matched according to the viRNAs described in the legend to Fig. 3 (see Table S1 in the supplemental material for details); hot- and cold-spot conservation was confirmed with other SFV viRNA distribution profiles from U4.4 or Aag2 cells, such as those shown in Fig. 4 and 5

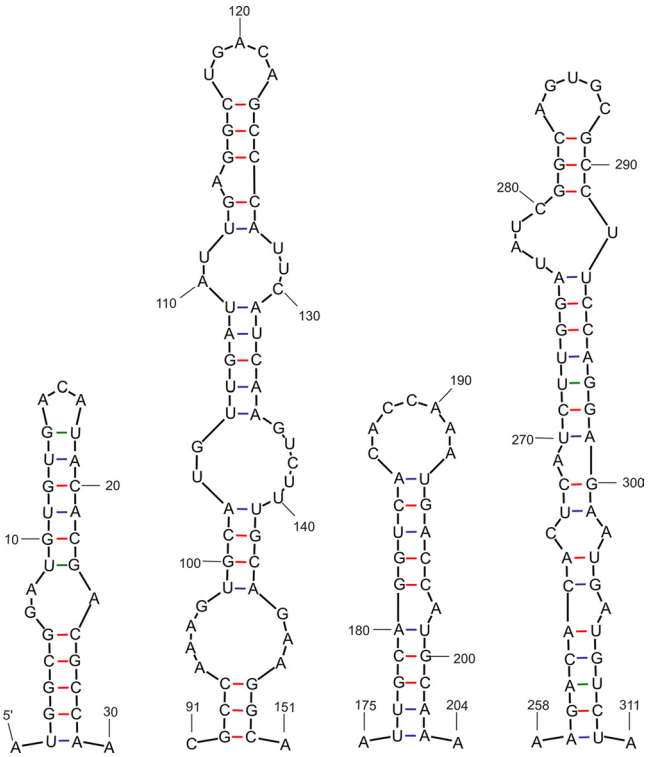

FIG. 7. RNA secondary structures in the 5′ region of the SFV4 genome, as predicted by Mfold. Numbers indicate positions of nucleotides in the SFV4 genome.

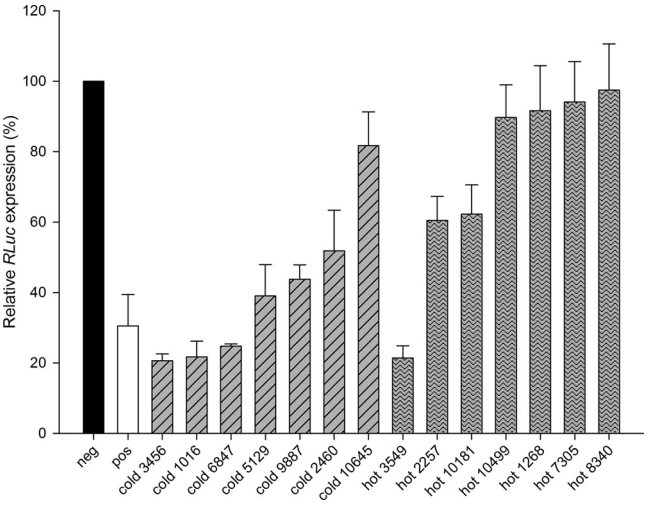

FIG. 8. Synthetic siRNA mimics of SFV genome hot-and cold-spot viRNAs (see Table 1 for details) and their effects on virus replication. *A. albopictus*-derived U4.4 cells were transfected with siRNAs (including a positive-control siRNA targeting *RLuc* [pos] and a negative-control scrambled siRNA [neg] [final concentration, 10 nM]) for 24 h and then infected with the reporter SFV4(3H)-*RLuc* (Fig. 1) at an MOI of 1. Following this step, *RLuc* activities (readout for SFV replication) were determined at 12 h p.i. and compared to that of negative-control scrambled siRNA (100% relative *RLuc* expression). Statistical analysis was performed by comparing the activities of hot- and cold-spot mimic siRNA groups ($P < 0.05$ by a Mann-Whitney U test). This experiment was performed in triplicate for each siRNA and repeated three times; bars show the average relative *RLuc* activities for each siRNA from all three experiments, and error bars represent standard errors.

(Table 1, and see Tables S2 and S3 in the supplemental material for details).

Biologically active viRNAs targeting the viral genome should mediate the degradation of viral RNA and thus reduce *RLuc* expression. U4.4 cells were transfected with siRNA mimics of hot- and cold-spot genome viRNAs (7 hot or cold spots; final concentration, 10 nM) for 24 h and then infected at an MOI of 1 with SFV4(3H)-*RLuc*, and *RLuc* activities were determined at 12 h p.i. As shown in Fig. 8, the overall ability of cold-spot viRNA mimics to inhibit SFV replication is significantly higher than that of hot-spot viRNA mimics ($P < 0.05$ by a statistical comparison of hot- and cold-spot-derived siRNA mimic activities by a Mann-Whitney U test). siRNA concentration ranges from 3.125 to 100 nM were tested for selected siRNAs, and siRNA mimics of viRNAs maintained their individual characteristics at various concentrations; i.e., siRNA mimics of hot-spot viRNAs generally displayed no or poor antiviral activity, while antivirally active siRNA mimics of cold-spot viRNAs also showed activity at 3.125 nM (data for three siRNA mimics of both hot- and cold-spot viRNAs as well as controls are shown in Fig. S3 in the supplemental material).

Experiments with siRNA mimics of hot- and cold-spot viRNAs were repeated with *A. aegypti*-derived Aag2 cells as described above, and the same effects were obtained (see Table 1 for comparison), with siRNA mimics of cold-spot viRNAs again being significantly more efficient than siRNA mimics of hot-spot viRNAs ($P < 0.05$ by a Mann-Whitney U test) at inhibiting SFV replication (Fig. 9). This demonstrates that our observations extend to cells derived from a related mosquito species.

DISCUSSION

RNAi is a major defense mechanism against arboviruses in mosquitoes (14, 38). However, surprisingly little is known about the dsRNA substrate for dicer and the origin of dsRNA-derived viRNAs which mediate the degradation of virus target RNA. To address this, we describe the application of deep-sequencing technology to SFV-infected *A. albopictus* U4.4 cells to characterize SFV-derived viRNAs produced during the acute phase of infection. Very noticeable hot spots of viRNA generation were identified along the length of the SFV genome and antigenome, while cold spots that generated no detectable or few viRNAs were also present. This is in agreement with previous findings with *A. aegypti* and *Anopheles gambiae* mosquitoes infected with alphaviruses and suggests that key features of alphavirus-induced antiviral RNAi are conserved within aedine and anopheline mosquitoes (38, 39). Moreover, similar viRNA distributions were observed for infections of mosquitoes with a flavivirus, West Nile virus (4). Together with a growing body of experimental evidence, our results support the hypothesis that alphaviruses do not encode, unlike many known insect-only viruses, protein-based RNAi inhibitors (14).

The nature of alphavirus-induced dsRNAs that give rise to viRNAs is not clear, although that is a key question in the

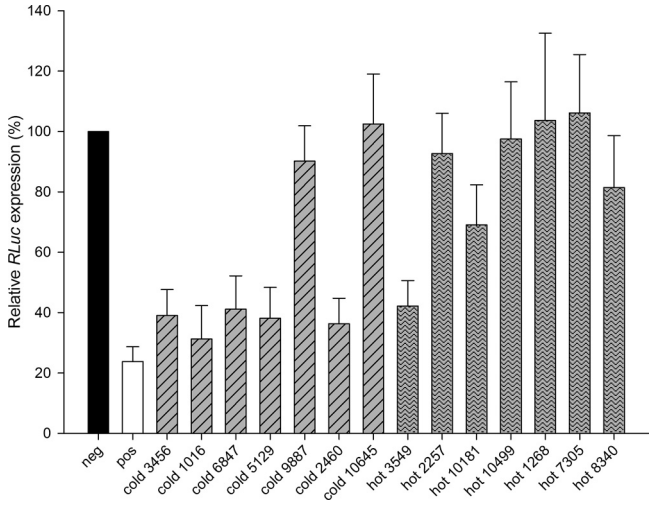

FIG. 9. Synthetic siRNA mimics of SFV genome hot- and cold-spot viRNAs (see Table 1 for details) and their effects on virus replication. *A. aegypti*-derived Aag2 cells were transfected with siRNAs (including a positive-control siRNA targeting *RLuc* [pos] and a negative-control scrambled siRNA [neg] [final concentration, 10 nM]) for 24 h and then infected with the reporter SFV4(3H)-*RLuc* (Fig. 1) at an MOI of 1. Following this step, *RLuc* activities (readout for SFV replication) were determined at 12 h p.i. and compared to that of negative-control scrambled siRNA (100% relative *RLuc* expression). Statistical analysis was performed by comparing the activities of hot- and cold-spot mimic siRNA groups ($P < 0.05$ by a Mann-Whitney U test). This experiment was performed in triplicate for each siRNA and repeated three times; bars show the average relative *RLuc* activities for each siRNA from all three experiments, and error bars represent standard errors.

understanding of viRNA distribution. One possibility is that, as with some plant viruses, RNA secondary structures could serve as substrates for dicer (20–22, 36). MFED and pairing analyses of the SFV genome delineate secondary structures at the 5′ end. The remainder of the genome contained only a few areas with a high probability of secondary structures. The lack of any correlation between the frequency of 21-nt viRNA production and regions of conserved base pairing indicates that the vast majority of viRNAs are not specifically targeted to genome secondary structures. Alphavirus viRNAs are therefore derived mainly from virus-induced dsRNAs, such as dsRNA replication intermediates, in line with a previously reported hypothesis (38); indeed, other arbovirus-derived small RNAs (resembling piwi-interacting RNAs [piRNAs]) in mosquito cells are prominent only in RNAi-deficient cell lines (5, 49). Although structures at the 3′ terminus of the flavivirus genome have been characterized in the past, these structures do not appear to be particularly targeted by the RNAi response or generate excess viRNAs during mosquito infection by West Nile virus (4). It therefore remains unclear how viRNAs are distributed into hot spots and cold spots. Areas that repeatedly generate hot-spot viRNAs may be in a conformation (pairing structures?) that favors the interaction with Dcr-2, although we did not observe a particular bias in dsRNA stability between hot-spot and cold-spot viRNAs by bioinformatics analysis (our unpublished observations). Those locations that generate few or no viRNAs (nonpairing structures?) may not favor those interactions, or cold spots could be shielded from the RNAi machinery. These two different conformations may work in opposite ways for target recognition by RISC, and hot-spot viRNAs would not silence SFV gene expression/replication as well as cold-spot viRNAs. The reason why hot-spot or cold-spot viRNAs do not uniquely act in the same way may also be due to the influence from tertiary and quaternary structures, as was described previously for siRNA targeting of hepatitis C virus (43). Our results with cold-spot viRNAs could also inform the choice of siRNAs as therapeutics against alphaviruses if similar findings are obtained for vertebrate cells.

Our results show that SFV does not inhibit the generation of viRNAs and that these viRNAs are generated in hot spots mainly along the SFV genome but also the antigenome. Presently, much information about the biology of viRNAs in insect cells stems from *D. melanogaster* flies and cells infected with a positive-strand RNA insect virus, flock house virus (FHV) (*Nodaviridae*) (1, 13, 56). In *D. melanogaster* cells latently infected with FHV, viRNAs are generated from dsRNA replication intermediates, which act as the main substrate for *Drosophila* Dcr-2 activity; again, viRNAs were derived from the entire FHV genome but with hot spots particularly at the 5′ ends of the bipartite FHV genome (13). We demonstrate that hot-spot-derived viRNAs, the predominant type of viRNA, are far less effective at silencing SFV replication than are cold-spot viRNAs. We suggest that alphaviruses, which do not appear to encode generally active suppressors of RNAi, might have evolved in this direction to produce decoy viRNAs that might hinder the RNAi machinery and allow the virus time to replicate before it is eventually silenced through RNAi. Hot-spot-derived viRNAs in *D. melanogaster* cells latently infected with FHV also display poor biological activities (13), similar to findings described in this study. In the case of FHV it was also found that the bulk of viRNAs were not loaded into Ago-2, which might account for the lack of silencing activity, although direct dicing of replication intermediates could also mediate antiviral activity (13). This might indeed suggest a genome nucleic acid-mediated resistance to RNAi, which allows limited replication without the need of a viral suppressor of RNAi (VSR). In particular, for alphaviruses, where the coexpression of powerful RNAi-inhibitory proteins has been shown to dramatically decrease mosquito survival, a viRNA-based decoy mechanism might be enough to maintain the delicate balance between arbovirus replication and vector survival (9, 39). At least in the case of a potato spindle tuber viroid, resistance to RNAi based solely on genome secondary structures has been identified; viroid-derived siRNAs stem mostly from secondary structures within the viroid RNA; however, these secondary structures are in turn highly resistant to RISC-mediated cleavage (22). Adenoviruses of vertebrates express RNAs that suppress RNAi (2, 31). West Nile virus appears to evade RNAi in vertebrate cells by making replication complexes inaccessible to the RNAi machinery, and similar evasion strategies have been suggested for alphaviruses (16, 18, 24); indeed, we showed (Fig. 2) that in the early acute phase, dsRNA is very closely associated with replication complexes. Strategies other than protein-based RNAi inhibitors may there-

fore be employed by arboviruses to limit the effects of mosquito antiviral RNAi responses.

ACKNOWLEDGMENTS

We declare no competing financial interests.

We thank R. Hernandez and D. T. Brown (North Carolina State University, Raleigh, NC) and P. Eggleston (Keele University, United Kingdom) for cells.

This work was supported by the Wellcome Trust (grant number 079699/Z/06/Z) (A.K.) and a BBSRC Roslin Institute Strategic Programme grant (J.K.F. and A.K.).

REFERENCES

1. **Aliyari, R., et al.** 2008. Mechanism of induction and suppression of antiviral immunity directed by virus-derived small RNAs in Drosophila. Cell Host Microbe **4:**387–397.
2. **Andersson, M. G., et al.** 2005. Suppression of RNA interference by adenovirus virus-associated RNA. J. Virol. **79:**9556–9565.
3. **Attarzadeh-Yazdi, G., et al.** 2009. Cell-to-cell spread of the RNA interference response suppresses Semliki Forest virus (SFV) infection of mosquito cell cultures and cannot be antagonized by SFV. J. Virol. **83:**5735–5748.
4. **Brackney, D. E., J. E. Beane, and G. D. Ebel.** 2009. RNAi targeting of West Nile virus in mosquito midguts promotes virus diversification. PLoS Pathog. **5:**e1000502.
5. **Brackney, D. E., et al.** 2010. C6/36 *Aedes albopictus* cells have a dysfunctional antiviral RNA interference response. PLoS Negl. Trop. Dis. **4:**e856.
6. **Brown, D. T.** 1984. Alphavirus growth in cultured vertebrate and invertebrate cells, p. 113–133. *In* M. A. Mayo and K. A. Herrop (ed.), Vectors in virus biology. Academic Press, New York, NY.
7. **Campbell, C. L., W. C. Black IV, A. M. Hess, and B. D. Foy.** 2008. Comparative genomics of small RNA regulatory pathway components in vector mosquitoes. BMC Genomics **9:**425.
8. **Campbell, C. L., et al.** 2008. *Aedes aegypti* uses RNA interference in defense against Sindbis virus infection. BMC Microbiol. **8:**47.
9. **Cirimotich, C. M., J. C. Scott, A. T. Phillips, B. J. Geiss, and K. E. Olson.** 2009. Suppression of RNA interference increases alphavirus replication and virus-associated mortality in *Aedes aegypti* mosquitoes. BMC Microbiol. **9:**49.
10. **Davey, M. W., and L. Dalgarno.** 1974. Semliki Forest virus replication in cultured Aedes albopictus cells: studies on the establishment of persistence. J. Gen. Virol. **24:**453–463.
11. **Davis, M., S. M. Sagan, J. P. Pezacki, D. J. Evans, and P. Simmonds.** 2008. Bioinformatic and physical characterizations of genome-scale ordered RNA structure in mammalian RNA viruses. J. Virol. **82:**11824–11836.
12. **Fazakerley, J. K., C. L. Cotterill, G. Lee, and A. Graham.** 2006. Virus tropism, distribution, persistence and pathology in the corpus callosum of the Semliki Forest virus-infected mouse brain: a novel system to study virus-oligodendrocyte interactions. Neuropathol. Appl. Neurobiol. **32:**397–409.
13. **Flynt, A., N. Liu, R. Martin, and E. C. Lai.** 2009. Dicing of viral replication intermediates during silencing of latent Drosophila viruses. Proc. Natl. Acad. Sci. U. S. A. **106:**5270–5275.
14. **Fragkoudis, R., G. Attarzadeh-Yazdi, A. A. Nash, J. K. Fazakerley, and A. Kohl.** 2009. Advances in dissecting mosquito innate immune responses to arbovirus infection. J. Gen. Virol. **90:**2061–2072.
15. **Fragkoudis, R., et al.** 2008. Semliki Forest virus strongly reduces mosquito host defence signaling. Insect Mol. Biol. **17:**647–656.
16. **Frolova, E. I., R. Gorchakov, L. Pereboeva, S. Atasheva, and I. Frolov.** 2010. Functional Sindbis virus replicative complexes are formed at the plasma membrane. J. Virol. **84:**11679–11695.
17. **Garoff, H., M. Sjoberg, and R. H. Cheng.** 2004. Budding of alphaviruses. Virus Res. **106:**103–116.
18. **Geiss, B. J., T. C. Pierson, and M. S. Diamond.** 2005. Actively replicating West Nile virus is resistant to cytoplasmic delivery of siRNA. Virol. J. **2:**53.
19. **Gould, E. A., et al.** 2010. Understanding the alphaviruses: recent research on important emerging pathogens and progress towards their control. Antiviral Res. **87:**111–124.
20. **Ho, T., D. Pallett, R. Rusholme, T. Dalmay, and H. Wang.** 2006. A simplified method for cloning of short interfering RNAs from *Brassica juncea* infected with Turnip mosaic potyvirus and Turnip crinkle carmovirus. J. Virol. Methods **136:**217–223.
21. **Ho, T., H. Wang, D. Pallett, and T. Dalmay.** 2007. Evidence for targeting common siRNA hotspots and GC preference by plant Dicer-like proteins. FEBS Lett. **581:**3267–3272.
22. **Itaya, A., et al.** 2007. A structured viroid RNA serves as a substrate for dicer-like cleavage to produce biologically active small RNAs but is resistant to RNA-induced silencing complex-mediated degradation. J. Virol. **81:**2980–2994.
23. **Kaariainen, L., and T. Ahola.** 2002. Functions of alphavirus nonstructural proteins in RNA replication. Prog. Nucleic Acid Res. Mol. Biol. **71:**187–222.
24. **Keene, K. M., et al.** 2004. RNA interference acts as a natural antiviral response to O'nyong-nyong virus (*Alphavirus*; Togaviridae) infection of *Anopheles gambiae*. Proc. Natl. Acad. Sci. U. S. A. **101:**17240–17245.
25. **Kemp, C., and J. L. Imler.** 2009. Antiviral immunity in Drosophila. Curr. Opin. Immunol. **21:**3–9.
26. **Khoo, C. H., J. Piper, I. Sanchez-Vargas, K. E. Olson, and A. W. Franz.** 2010. The RNA interference pathway affects midgut infection- and escape barriers for Sindbis virus in *Aedes aegypti*. BMC Microbiol. **10:**130.
27. **Kiiver, K., et al.** 2008. Properties of non-structural protein 1 of Semliki Forest virus and its interference with virus replication. J. Gen. Virol. **89:**1457–1466.
28. **Kulasegaran-Shylini, R., S. Atasheva, D. G. Gorenstein, and I. Frolov.** 2009. Structural and functional elements of the promoter encoded by the 5′ untranslated region of the Venezuelan equine encephalitis virus genome. J. Virol. **83:**8327–8339.
29. **Li, R., Y. Li, K. Kristiansen, and J. Wang.** 2008. SOAP: short oligonucleotide alignment program. Bioinformatics **24:**713–714.
30. **Logue, C. H., B. J. Sheahan, and G. J. Atkins.** 2008. The 5′ untranslated region as a pathogenicity determinant of Semliki Forest virus in mice. Virus Genes **36:**313–321.
31. **Lu, S., and B. R. Cullen.** 2004. Adenovirus VA1 noncoding RNA can inhibit small interfering RNA and microRNA biogenesis. J. Virol. **78:**12868–12876.
32. **Lulla, A., V. Lulla, K. Tints, T. Ahola, and A. Merits.** 2006. Molecular determinants of substrate specificity for Semliki Forest virus nonstructural protease. J. Virol. **80:**5413–5422.
33. **Mathews, D. H., J. Sabina, M. Zuker, and D. H. Turner.** 1999. Expanded sequence dependence of thermodynamic parameters improves prediction of RNA secondary structure. J. Mol. Biol. **288:**911–940.
34. **Merits, A., L. Vasiljeva, T. Ahola, L. Kaariainen, and P. Auvinen.** 2001. Proteolytic processing of Semliki Forest virus-specific non-structural polyprotein by nsP2 protease. J. Gen. Virol. **82:**765–773.
35. **Miller, M. L., and D. T. Brown.** 1992. Morphogenesis of Sindbis virus in three subclones of *Aedes albopictus* (mosquito) cells. J. Virol. **66:**4180–4190.
36. **Molnar, A., et al.** 2005. Plant virus-derived small interfering RNAs originate predominantly from highly structured single-stranded viral RNAs. J. Virol. **79:**7812–7818.
37. **Monath, T. P.** 1994. Dengue: the risk to developed and developing countries. Proc. Natl. Acad. Sci. U. S. A. **91:**2395–2400.
38. **Myles, K. M., E. M. Morazzani, and Z. N. Adelman.** 2009. Origins of alphavirus-derived small RNAs in mosquitoes. RNA Biol. **6:**1–5.
39. **Myles, K. M., M. R. Wiley, E. M. Morazzani, and Z. N. Adelman.** 2008. Alphavirus-derived small RNAs modulate pathogenesis in disease vector mosquitoes. Proc. Natl. Acad. Sci. U. S. A. **105:**19938–19943.
40. **Nickens, D. G., and R. W. Hardy.** 2008. Structural and functional analyses of stem-loop 1 of the Sindbis virus genome. Virology **370:**158–172.
41. **Ou, J. H., E. G. Strauss, and J. H. Strauss.** 1983. The 5′-terminal sequences of the genomic RNAs of several alphaviruses. J. Mol. Biol. **168:**1–15.
42. **Pialoux, G., B. A. Gauzere, S. Jaureguiberry, and M. Strobel.** 2007. Chikungunya, an epidemic arbovirosis. Lancet Infect. Dis. **7:**319–327.
43. **Sagan, S. M., N. Nasheri, C. Luebbert, and J. P. Pezacki.** 2010. The efficacy of siRNAs against hepatitis C virus is strongly influenced by structure and target site accessibility. Chem. Biol. **17:**515–527.
44. **Saleh, M. C., et al.** 2009. Antiviral immunity in Drosophila requires systemic RNA interference spread. Nature **458:**346–350.
45. **Salonen, A., T. Ahola, and L. Kaariainen.** 2005. Viral RNA replication in association with cellular membranes. Curr. Top. Microbiol. Immunol. **285:**139–173.
46. **Sanchez-Vargas, I., et al.** 2009. Dengue virus type 2 infections of *Aedes aegypti* are modulated by the mosquito's RNA interference pathway. PLoS Pathog. **5:**e1000299.
47. **Sanchez-Vargas, I., et al.** 2004. RNA interference, arthropod-borne viruses, and mosquitoes. Virus Res. **102:**65–74.
48. **Schonborn, J., et al.** 1991. Monoclonal antibodies to double-stranded RNA as probes of RNA structure in crude nucleic acid extracts. Nucleic Acids Res. **19:**2993–3000.
49. **Scott, J. C., et al.** 2010. Comparison of dengue virus type 2-specific small RNAs from RNA interference-competent and -incompetent mosquito cells. PLoS Negl. Trop. Dis. **4:**e848.
50. **Simmonds, P., et al.** 2008. Bioinformatic and functional analysis of RNA secondary structure elements among different genera of human and animal caliciviruses. Nucleic Acids Res. **36:**2530–2546.
51. **Simmonds, P., A. Tuplin, and D. J. Evans.** 2004. Detection of genome-scale ordered RNA structure (GORS) in genomes of positive-stranded RNA viruses: implications for virus evolution and host persistence. RNA **10:**1337–1351.
52. **Spuul, P., et al.** 2007. Role of the amphipathic peptide of Semliki Forest virus replicase protein nsP1 in membrane association and virus replication. J. Virol. **81:**872–883.
53. **Stollar, V., T. E. Shenk, and B. D. Stollar.** 1972. Double-stranded RNA in hamster, chick, and mosquito cells infected with Sindbis virus. Virology **47:**122–132.
54. **Strauss, J. H., and E. G. Strauss.** 1994. The alphaviruses: gene expression, replication, and evolution. Microbiol. Rev. **58:**491–562.
55. **Tamberg, N., et al.** 2007. Insertion of EGFP into the replicase gene of Semliki Forest virus results in a novel, genetically stable marker virus. J. Gen. Virol. **88:**1225–1230.

56. **van Rij, R. P., and E. Berezikov.** 2009. Small RNAs and the control of transposons and viruses in Drosophila. Trends Microbiol. **17:**163–171.
57. **Varjak, M., E. Zusinaite, and A. Merits.** 2010. Novel functions of the alphavirus nonstructural protein nsP3 C-terminal region. J. Virol. **84:** 2352–2364.
58. **Weaver, S. C.** 2006. Evolutionary influences in arboviral disease. Curr. Top. Microbiol. Immunol. **299:**285–314.
59. **Weaver, S. C., and A. D. Barrett.** 2004. Transmission cycles, host range, evolution and emergence of arboviral disease. Nat. Rev. Microbiol. **2:**789–801.
60. **Weber, F., V. Wagner, S. B. Rasmussen, R. Hartmann, and S. R. Paludan.** 2006. Double-stranded RNA is produced by positive-strand RNA viruses and DNA viruses but not in detectable amounts by negative-strand RNA viruses. J. Virol. **80:**5059–5064.
61. **Yoo, B. C., et al.** 2004. A systemic small RNA signaling system in plants. Plant Cell **16:**1979–2000.
62. **Zuker, M.** 2000. Calculating nucleic acid secondary structure. Curr. Opin. Struct. Biol. **10:**303–310.
63. **Zuker, M.** 2003. Mfold Web server for nucleic acid folding and hybridization prediction. Nucleic Acids Res. **31:**3406–3415.